Journal of Materials Chemistry A

Accepted Manuscript

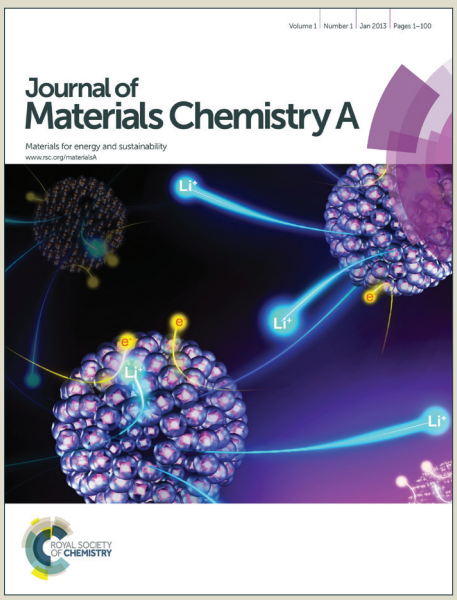

ROYAL SOCIETY OF CHEMISTRY

www.rsc.org/materialsA

Journal of

Materials Chemistry A

RSCPublishing

PAPER

In-situ polyaniline modified cathode material $Li[Li_{0.2}Mn_{0.54}Ni_{0.13}Co_{0.13}]O_2$ with high rate capacity for lithium ion batteries

Qingrui. Xue,[a] Jianling. Li,[*a] Guofeng. Xu,[a] Hongwei. Zhou,[a] Xindong. Wang[a], Feiyu. Kang[b]

Cite this: DOI: 10.1039/x0xx00000x

Received 00th January 2012,
Accepted 00th January 2012

DOI: 10.1039/x0xx00000x

www.rsc.org/

Lithium-rich layered $Li[Li_{0.2}Mn_{0.54}Ni_{0.13}Co_{0.13}]O_2$ is prepared by a fast co-precipitation method, and surface modified with conducting polyaniline (PANI, 5 wt%, 10 wt%, 15 wt%, 20 wt%, 30 wt% theoretically) via in-situ chemical oxidation polymerization to optimize the electrochemical properties. The uniform PANI layer with the thickness of 5 nm (10 wt%) has been successfully coated on the surface of $Li[Li_{0.2}Mn_{0.54}Ni_{0.13}Co_{0.13}]O_2$ particles, as observed by field-emission scanning electron microscopy(FESEM) and high resolution transmission electron microscope(HRTEM). The X-ray powder diffraction (XRD) results show that all of the prepared samples have a typical layered hexagonal α-$NaFeO_2$ structure. The PANI layer maintains the integrity of surface material crystal structure of the $Li[Li_{0.2}Mn_{0.54}Ni_{0.13}Co_{0.13}]O_2$ particles by protecting the electrodes from external erosion in the continuous charge-discharge cycles. PANI-coated $Li[Li_{0.2}Mn_{0.54}Ni_{0.13}Co_{0.13}]O_2$ electrodes present excellent electrochemical properties at room temperature. The initial discharge capacity is 313.5 mA h g^{-1} (0.05 C) with the coulombic efficiency of 89.01% (PANI, 10 wt%), compared with 291.9 mA h g^{-1} (0.05 C) for the pristine $Li[Li_{0.2}Mn_{0.54}Ni_{0.13}Co_{0.13}]O_2$ with the coulombic efficiency of 81.31% in the potential range 2.0–4.8 V (*vs*. Li/Li^+). The discharge capacity retains at 273.5 mA h g^{-1} after 100 cycles at 0.1 C. Meanwhile, the PANI-coated $Li[Li_{0.2}Mn_{0.54}Ni_{0.13}Co_{0.13}]O_2$ exhibits excellent high rate capacity of 198.6 mA h g^{-1} at 10 C. The electrochemical impedance spectra (EIS) measurements reveal that the thin PANI coating layer optimizes the interfacial electrochemical reaction activity greatly by reducing the charge transfer resistance. Moreover, the special H^+/Li^+ exchange reaction during the proton acid doping procedure promotes the improvement of electrochemical performance as well.

Introduction

As the portable energy storage and conversion device, batteries have reshaped our concept of energy consumption in the past decades. The rechargeable lithium-ion batteries (LIBs) are considered as the most advanced energy supplying device for the mobile electronics, electric vehicles (EVs) and hybrid electric vehicles (HEVs).[1-4] However, the available LIBs are increasingly unable to meet the changing requirements due to the limited electrochemical performance of the commercial cathode materials, such as poor energy density ($LiCoO_2$, 140 mA h g^{-1}),[5,6] low conductivity of electron/lithium-ion diffusivity ($LiFePO_4$)[7-9] and the structural vulnerability ($LiMn_2O_4$).[10-12] Therefore, it is significant to search for high voltage, low cost, safe, high energy density and good high rate capability cathodes for the advanced LIBs.

With the deepening of research on cathode materials, a new family of lithium-rich layered solid solution cathode materials $xLi_2MnO_3 \cdot (1\text{-}x)\ LiMO_2$ (M=Mn, Co, Ni, etc) have attracted great interests due to their low cost, high voltage (4.8 V *vs* Li/Li^+) and theoretical capacity (over 250 mA h g^{-1}).[13-16] It has been reported that the initial electrochemical reaction mechanism has great influence on the electrochemical performance of the solid solution cathodes in the following cycles. Based on the layered hexagonal α-$NaFeO_2$ structure, $Li[Li_{0.2}Mn_{0.54}Ni_{0.13}Co_{0.13}]O_2$ is consisted of two components $LiMn_{1/3}Ni_{1/3}Co_{1/3}O_2$ (space group $R\bar{3}m$) and Li_2MnO_3 (space group $C/2m$).[17,18] During the initial charge process, lithium ion deintercalates continuously from $LiMn_{1/3}Ni_{1/3}Co_{1/3}O_2$ accompanying with the oxidation of the transition metals below 4.5 V (*vs* Li/Li^+).[19] A plateau will be formed between 4.4 V and 4.6 V as the result of lithium ion deintercalating from the octahedral

interspace of Li_2MnO_3 accompanying with oxygen releasing in the form of Li_2O.[20] However, the special deintercalation way of lithium ion provides $Li[Li_{0.2}Mn_{0.54}Ni_{0.13}Co_{0.13}]O_2$ with high charge capacity, as well as induces large irreversible capacity loss caused by the inherent properties of Li_2MnO_3, such as the irreversible oxygen release, ion rearrangement, excitation and dissolution of transition metal and poor conducting performance,[21-23] which lead to the low coulombic efficiency in the initial cycle, poor rate capacity, and safety hazard due to the reactive oxygen.

In order to optimize the electrochemical properties of $xLi_2MnO_3\cdot(1-x)LiMO_2$, the damages to the structure and active ingredient must be suppressed during the continuous cycles. In recent researches, strategies of surface modification,[24-26] cation doping or replacement at Mn sites,[27,28] compositing with other electrode materials[29] and acid treatment[30,31] have been explored to improve the capacity, coulombic efficiency, high rate capability and cycle stability. The surface modification with electro-active materials ($Li_4Ti_{12}O_5$, $LiMnPO_4$, $LiNiPO_4$, and MnO_2) and high conductive materials (C, Al_2O_3, ZrO_2, Sm_2O_3 and Bi_2O_3) proved to be effective in reducing the electrochemical resistance and improving electrochemical performance.[32-40] Kim *et al*[41] and Xu *et al*[42] reported that the special H^+/Li^+ exchange during the acid treatment contributed to the high capacity and cycle stability by enhancing the reduction ability of oxygen and stabilizing the electrode surface. However, the conventional modification can hardly provide improvements both in the initial electrochemical properties and the continuous cycle stability. Thus, it is a feasible way to explore the compound modification of surface coating and acid treatment for the development of high energy density cathode materials.

Conductive polymer PANI has been proposed as a strategy of improving electrical conductivity for the poor conducting cathode materials due to its high electrochemical stability, facile synthesis, controlled electrochemical performance by protonation and high electrical conductivity.[43-45] In addition, the active electrode materials $LiMn_2O_4$,[46] $Li(Mn_{1/3}Ni_{1/3}Fe_{1/3})O_2$,[47] MnO_2[48] or graphene[49] that composited with PANI present excellent electrochemical properties for the lithium battery and supercapacitor. In this work, PANI is introduced as a conductive coating layer by in-situ polymerizing on the surface of Li-rich layered $Li[Li_{0.2}Mn_{0.54}Ni_{0.13}Co_{0.13}]O_2$. Especially, we extend the proton process in order to induce the H^+/Li^+ exchange reaction occurring on the surface of the prepared particles. The synergetic effects of PANI surface coating and acid treatment are expected to stabilize interface structure, reduce the electrochemical resistance and improve the electrochemical performance of the pristine $Li[Li_{0.2}Mn_{0.54}Ni_{0.13}Co_{0.13}]O_2$.

Experimental

Synthesis of the materials

The nanomaterial $Li[Li_{0.2}Mn_{0.54}Ni_{0.13}Co_{0.13}]O_2$ was prepared by a fast co-precipitation method.[50] Mixed aqueous solution (2 M) of $NiSO_4\cdot6H_2O$, $CoSO_4\cdot7H_2O$ and $MnSO_4\cdot H_2O$ was co-precipitated with KOH and $NH_3\cdot H_2O$ as the precipitant in the stirred reaction tank. The reaction PH value was controlled between 11 and 12 under the shielding atmosphere of argon. Sulfate ions in the precipitate were filtered out by distilled deionized water 5 min later and the synthesized precipitates were dried in the vacuum oven at 120 °C for 12 h. The dried precursor was ground with $LiOH\cdot H_2O$ which was 5 wt% excess in stoichiometric ratio, and then preheated at 450 °C for 1 h. After the high temperature calcination at 950 °C for 24 h, the particles were quenched with liquid nitrogen.

Aniline was polymerized on the surface of $Li[Li_{0.2}Mn_{0.54}Ni_{0.13}Co_{0.13}]O_2$ particles using the method of in-situ chemical oxidation polymerization with protonation as proton acid doping agent. 1 g of the prepared $Li[Li_{0.2}Mn_{0.54}Ni_{0.13}Co_{0.13}]O_2$ was ultrasonically dispersed into 100 ml distilled deionized water for 45 min, then controlled the PH value between 2 and 3 with the addition of hydrochloric acid (1 M) in the stirred reaction tank. Being stirred for 1 h at room temperature, the distilled aniline with the specific percentage (5 wt%, 10 wt%, 15 wt%, 20 wt% and 30 wt% theoretically) was pumped into the turbid liquid under the shielding atmosphere of argon. In the chemical polymerization process, ammonium persulfate in the molar ratio of 1:1 with aniline was added into the aniline solution drop by drop. Following by the polymerize reaction for 6 h in ice bath, the green solution was filtered by air pump filtration with distilled deionized water several times, and then dried in the vacuum oven at 75 °C for 15 h. The schematic of synthesis process is shown in Fig. 1.

Characterizations of the materials

The real aniline polymerization amount that coated on the surface of $Li[Li_{0.2}Mn_{0.54}Ni_{0.13}Co_{0.13}]O_2$ was measured by thermogravimetric analysis (TGA, TA Instruments DMA2980) at the heating rate of 10 °C min^{-1} under pure oxygen atmosphere. The corresponding real coating amount were 1.38 wt%, 1.81 wt%, 2.28 wt%, 2.64 wt%, and 3.6 wt%, respectively(Fig. S1†). The crystalline structures of the prepared samples were analyzed by X-ray powder diffraction (XRD, Rigaku TTRⅢ) using Cu Kα radiation at 2θ=10°-80°

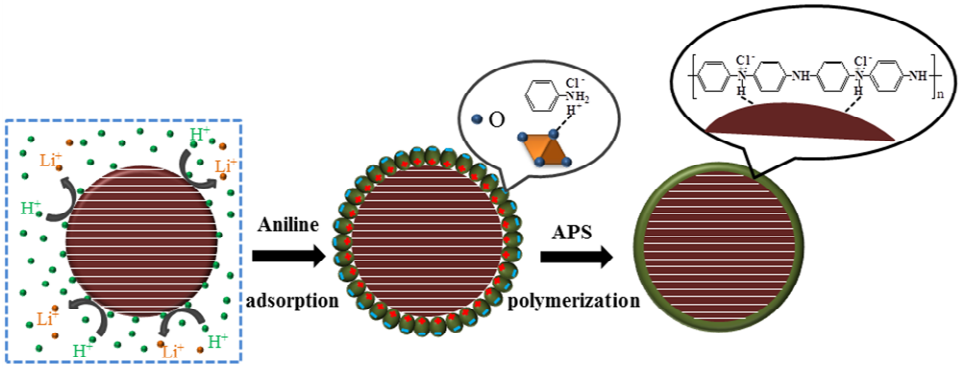

Fig. 1 Synthesis schematic of the PANI-coated $Li[Li_{0.2}Mn_{0.54}Ni_{0.13}Co_{0.13}]O_2$.

with the scanning rate of 3° min^{-1}. The morphology observation of the particles was carried out by field-emission scanning electron microscopy (FESEM, Zeiss SUPRATM 55), transmission electron microscope (TEM, FEI Tecnai F30), high resolution transmission electron microscope (HRTEM, FEI Tecnai F30) and energy-dispersive x-ray spectroscopy (EDS, Sigma Kevex Superdry). The relative contents of Li, Ni, Co, and Mn in the prepared samples were monitored by inductively coupled plasma-atomic emission spectrometry (ICP-AES, Perkin Optima 7000DV) analyses.

Electrochemical measurements

The electrochemical properties were tested by galvanostatic cycling using CR2025 coin cells. The working electrode slurry was smeared on the current collector of aluminum foil by the method of doctor blade, consisting of the prepared active material (75 wt%), conductive carbon black (15 wt%) and polyvinylidene fluoride (10 wt%), and then dried in the vacuum drying oven at 80 °C for 15 h. $LiPF_6$ (1 M) that dissolved in ethylene carbonate (EC) and dimethyl carbonate (DMC) with the volume ratio of 1:1 was used as electrolyte, Celgard 2400 membrane as the separator. The assembly of the coin cells was completed in the glove box which was filled with argon. Galvanostatic cycling studies were performed under the cut-off potential of 2.0 V and 4.8 V (*vs.* Li/Li^+) at different charge-discharge current densities using the Land battery test system (LANHE CT2001A). Electrochemical impedance spectroscopy was recorded by VMP2 electrochemical station (Princeton Applied Research VersaSTAT3) at room temperature between 1 MHz and 10 mHz with the amplitude of 10 mVrms.

Results and discussion

Structure and morphology

The XRD patterns of the pristine $Li[Li_{0.2}Mn_{0.54}Ni_{0.13}Co_{0.13}]O_2$ (labelled: LNCM) and the modified $Li[Li_{0.2}Mn_{0.54}Ni_{0.13}Co_{0.13}]O_2$ with PANI in different molar ratios (short for PI1/5 wt%, PI2/10 wt%, PI3/15 wt%, PI4/20 wt%, PI5/30 wt%) are shown in Fig. 2. All of the diffraction peaks can be indexed according to the layered α-$NaFeO_2$ structure with the space group $R\bar{3}m$ layered symmetry,[51] except for the special weak lattice reflections (space group *C/2m*) between 20° and 23° signed by the red narrows. The weak reflections are typically caused by the super-lattice ordering the transition metal ions and Li^+ in the transition metal layer.[52,53] Good crystallinity has been proved by the sharp diffraction peaks. Particularly, the splits between the adjacent peaks of (006)/(012), (108)/(110) and the ratio of $I_{(003)/(104)}$>1.2 indicate great two-dimensional layered structure and low cation disorder occurred between Li^+ and Ni^{2+}.[54] Rietveld refinement unit cell parameters of the pristine LNCM and PANI coated-LNCM are shown in Table 1. In general, surface modification has no effect on thelattice parameters of the pristine material, while the increasing value of *c* could be induced by the special acid leaching during proton acid doping procedure. The relative contents of Li, Ni, Co, and Mn in LNCM and PI2 are presented in Table 2. Obviously, the experimental chemical composition is in good agreement with the theoretical value, and the Li content decreases from 1.216 to 1.176 during the acid leaching. The reduction in intensity of the peaks (020) and (110) indicates that H^+/Li^+ exchange reaction comes from the Li_2MnO_3 component.[55] The diffusion path of Li^+ that facilitated by tetrahedral interslab space can be calculated based on the following equations.[56]

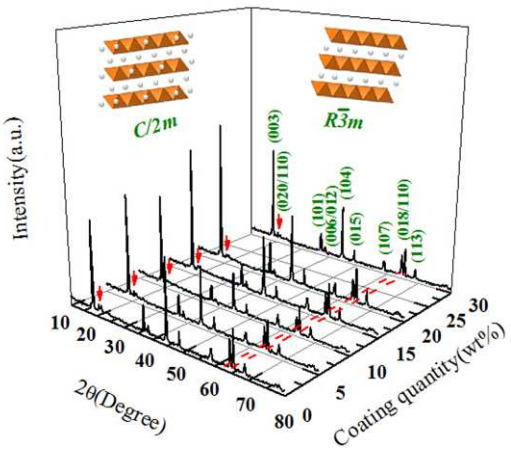

Fig. 2 XRD patterns of the prepared samples.

$$S_{NiO_2} = \left(\frac{2}{3} - 2Z_{OX}\right) \cdot C_{hex} \quad (1)$$

$$I_{LiO_2} = \frac{C_{hex}}{3} - S_{NiO_2} \quad (2)$$

In which Z_{OX}=0.2411, C_{hex}=*c*, S_{NiO_2} and I_{LiO_2} represent interslab distance of NiO_2 and LiO_2.[57] The resistance of internal Li^+ diffusion is strongly restricted by the Li slab distance. After the acid treatment, the effect on the interslab space between the cubic closed-packed oxide ion layers has optimized the diffusion path of Li^+ (Fig. 3). As we can see, PI2 presents the best ability of internal Li^+ diffusion with the increased Li slab distance.

Table 1 Rietveld refinement unit cell parameters of the prepared samples.

Samples	LNCM	PI1	PI2	PI3	PI4	PI5
a (nm)	0.285494	0.285494	0.285494	0.285494	0.285494	0.285494
c (nm)	1.425371	1.426318	1.429420	1.427536	1.426017	1.42556
c/*a*	4.99264	4.99597	5.00683	5.00231	4.99264	4.96179
V(nm^3)	0.1006	0. 1007	0. 1009	0. 1006	0.1007	0.1000

Table 2 The relative amounts of Li, Ni, Co, and Mn in the pristine LNCM and PI2.

Samples	Li	Ni	Co	Mn
Theoretial sample	1.200	0.130	0.130	0.540
LNCM	1.216	0.127	0.130	0.540
PI2	1.176	0.127	0.130	0.540

FT-IR spectra were tested to prove the existence of PANI on the surface of the PANI-coated sample and investigate the interfacial interaction between PANI coating layer (PI2) and $Li[Li_{0.2}Mn_{0.54}Ni_{0.13}Co_{0.13}]O_2$ particles (Fig. 4). The characteristic bands at 1580 cm^{-1}, 1490 cm^{-1}, 1310 cm^{-1}, 1245 cm^{-1} and 1140 cm^{-1} observed in PANI sample (Fig. 4b) are attributed to C=C stretching vibrations in the quinoid ring (Q-band), C-C stretching vibrations of the benzenoid ring (B-band), N-B-N stretching vibrations, C-NH^+ stretching vibrations and bending modes for the benzenoid unit, respectively.[58,59] For the PANI-coated sample, the Q-band is shifted to higher wavenumber (1631 cm^{-1}), and the intensity of C-NH^+ band (1310 cm^{-1}) is weakened, which can be interpreted by the special interaction between PANI and the transition metal oxide surface.[60] It could be expected that, the doped PANI will enhance the electronic conduction of the layered $Li[Li_{0.2}Mn_{0.54}Ni_{0.13}Co_{0.13}]O_2$ in the electrochemical reaction due to its high electrical conductivity.

FESEM images of the pristine LNCM and PANI coated-LNCM samples are shown in Fig. 5. It can be seen that the particle size of LNCM is in the range of 100 nm-200 nm, and there are no changes in micro-morphology and particle size after the surface modification with PANI in low amounts, as presented in Fig. 5b (PI1) and Fig. 5c (PI2). The distinct crystal faces and boundaries demonstrate good crystallinity of the LNCM particles indirectly. With the increase of coating amounts, fragmentary polyaniline slices appear among the crystal boundaries and the smooth particle surface become more and more rough, then leading to slight agglomeration. The element distributions on the surface of PI2 are monitored by energy-dispersive x-ray spectroscopy (Fig. 6). There exists acceptable error in the identification results under the resolution limit of 130 eV (using Mn, Ka radation), however the

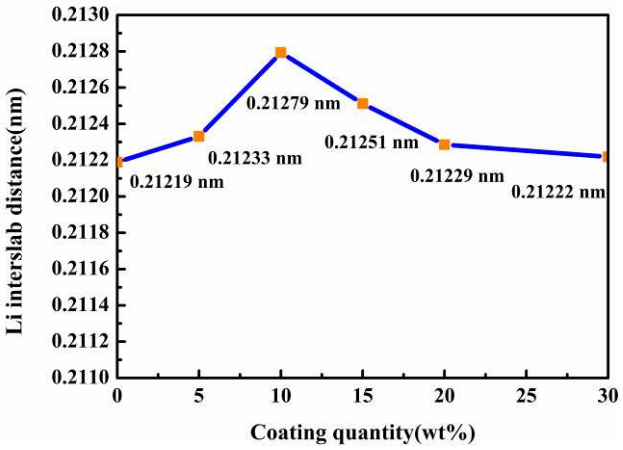

Fig. 3 Li slab distance of the prepared samples.

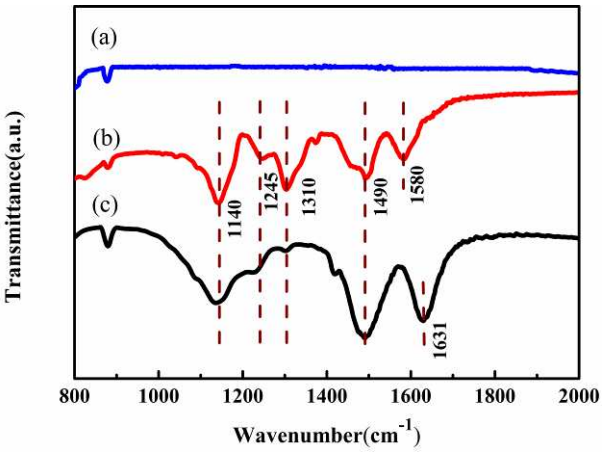

Fig. 4 FT-IR spectra of (a) the pristine LNCM, (b) PANI and (c) PI2.

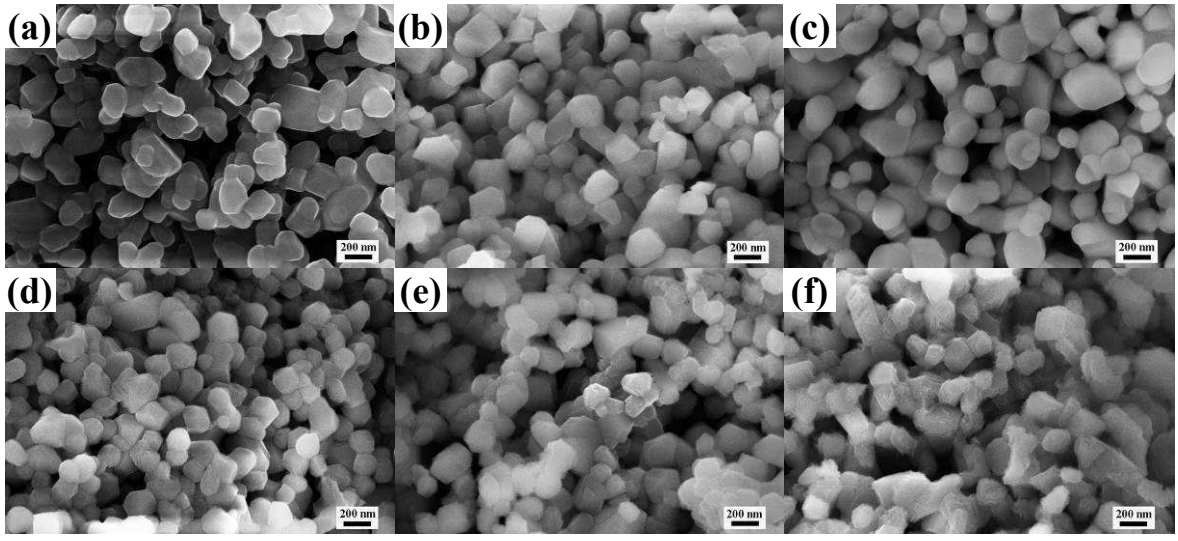

Fig. 5 SEM images of the prepared samples: (a) the pristine LNCM, (b) PI1, (c) PI2, (d) PI3, (e) PI4 and (f) PI5.

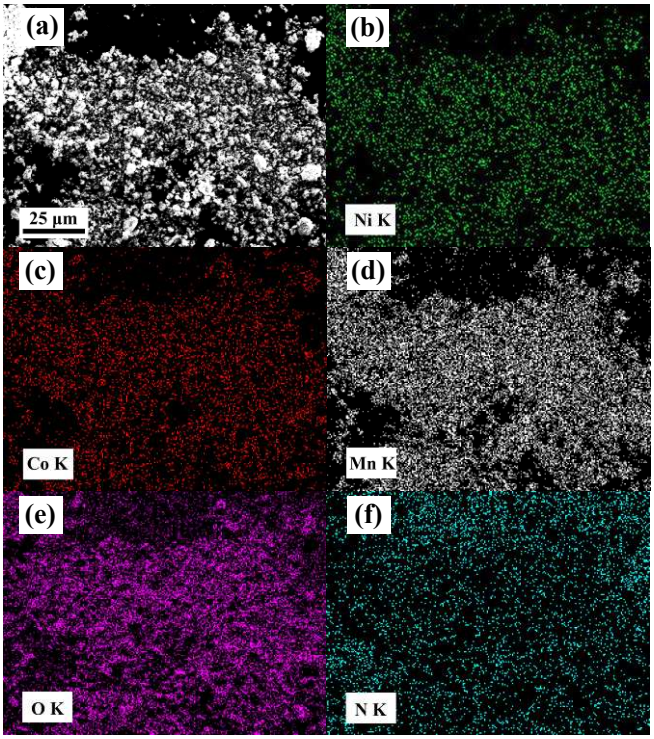

Fig. 6 The elements mapping of PI2: (a) PI2, (b) Ni, (c) Co, (d) Mn, (e) O and (f) N.

qualitative uniform distributions of Mn, Ni, Co, and O indicate that the in-situ chemical oxidation polymerization coating do not induce surface elements damage of MO_2 (M=Ni, Co, Mn).

For surface modification, thickness of the coating layer is an important evaluation factor. The coating layer with appropriate thickness will ensure excellent lithium ion transfer ability as well as stabilize the interface between electrode and electrolyte. In order to observe further morphology, microstructure of the pristine LNCM and PANI-coated LNCM were investigated by TEM and HRTEM, as shown in Fig. 7. Obviously, the ultra-thin and uniform PANI coating layer with the thickness of about 5 nm is formed successfully on the surface of $Li[Li_{0.2}Mn_{0.54}Ni_{0.13}Co_{0.13}]O_2$ particles (Fig. 7e, 7f) based on the FT-IR results (Fig. 4) and elements mapping results (Fig. 6f). TEM images clearly show that the individually dispersed particles become slightly agglomerate with superabundant aniline polymerizing on the surface of $Li[Li_{0.2}Mn_{0.54}Ni_{0.13}Co_{0.13}]O_2$ particles (Fig. S2†). Further, the straight and continuous fringes corresponding to typical layered (003) plane of $R\bar{3}m$ demonstrate that there are no crystal form transfers on the surface of the particle before and after PANI coating.

Electrochemical performance

For lithium-rich solid solution cathode material LNCM, the initial charge-discharge cycle plays a key role in the following electrochemical performance. To investigate the effects of PANI coating layer on the very initial charge-discharge performance, the cells were tested at low rate (0.05 C) in the potential range 2.0-4.8 V (*vs* Li/Li^+), as shown in Fig. 8. The similar curves present two obvious charge phases: the first stage that lithium ion deintercalates continuously from $LiMO_2$ (M = $Ni_{1/3}Co_{1/3}Mn_{1/3}$, space group $R\bar{3}m$) accompanying with the oxidation of the transition metals below 4.5V as expressed by Eq. 3; the second stage that shown as a plateau between 4.4 V and 4.6 V relates to the deintercalation of lithium ion from the octahedral interspace of Li_2MnO_3 (*C/2m*) accompanying with oxygen releasing in the form of Li_2O (Eq. 4).[35] The special deintercalation patterns of lithium ion provide $Li[Li_{0.2}Mn_{0.54}Ni_{0.13}Co_{0.13}]O_2$ with high charge capacity, as well as lead to the large irreversible capacity loss, because the oxygen ion vacancies are partly occupied by the transition metal.[61]

$$xLi_2MnO_3\cdot(1-x)LiMO_2 \rightarrow xLi_2MnO_3\cdot(1-x)MO_2 + (1-x)Li^+ + (1-x)e^- \quad (3)$$

$$xLi_2MnO_3\cdot(1-x)MO_2 \rightarrow xMnO_2\cdot(1-x)MO_2 + xLi_2O + 2xe^- \quad (4)$$

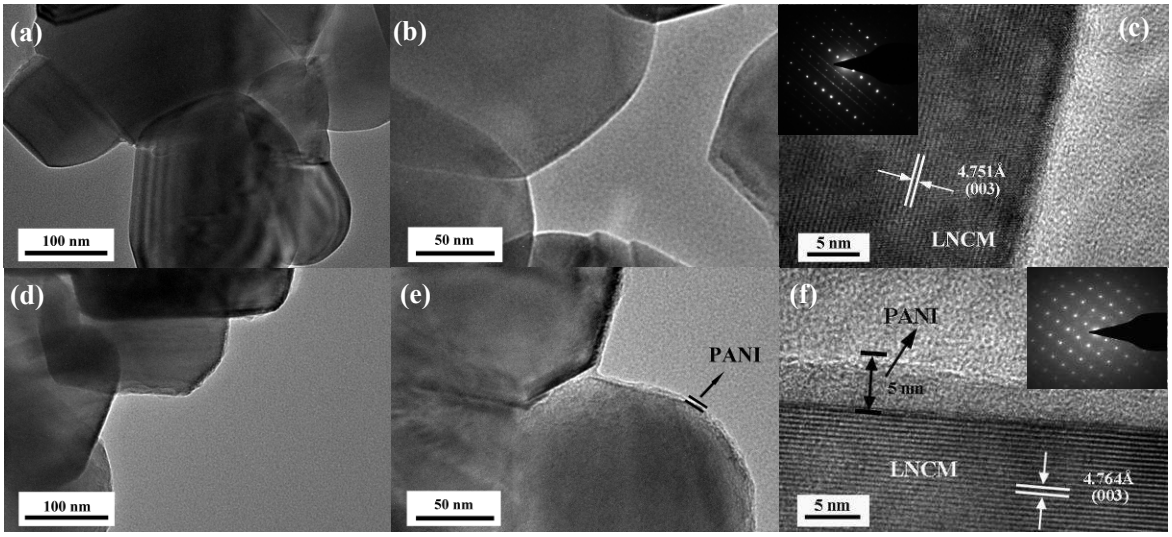

Fig. 7 TEM images of (a),(b) the pristine LNCM and (d), (e) PI2, HRTEM images of (c) the pristine LNCM and (f) PI2 (inset: electron diffraction patterns).

The pristine LNCM has an initial charge capacity of 359.0 mA h g^{-1} exceeding to its theoretical value, while PANI-coated LNCM deliver a lower initial charge capacity of 349.1 mA h g^{-1}, 352.2 mA h g^{-1}, 354.2 mA h g^{-1}, 350.4 mA h g^{-1} and 353.5 mA h g^{-1} for PI1, PI2, PI3, PI4 and PI5, respectively. However, higher initial coulombic efficiencies are obtained for the PANI-coated electrodes as represented in Fig. 9a. In particular, the electrode PI2 exhibits the highest coulombic efficiency of 89.01% in comparison with 81.31% of the pristine electrode. To explore the reasons of the anomalous initial electrochemical performance of the PANI-coated LNCM, the detailed charge information under different potential ranges before and after PANI coating is discussed (Table 3). It is clear that all of the PANI-coated LNCM exhibit lower charge capacity between 4.4 V and 4.6 V (*vs* Li/Li^+), than that of the pristine LNCM, indicating that lithium ion deintercalation (Eq. 4) is partly suppressed by the PANI coating layer. For the range of 2-4.4 V (*vs* Li/Li^+), there is almost no difference in the charge capacity. Therefore, the inhibitory effect on lithium ion deintercalating from the octahedral interspace of Li_2MnO_3 (*C*/2*m*) and the loss of lithium ion (Table 2) during the H^+/Li^+ exchange reaction lead to the ultimate capacity loss. According to our previous research, H^+/Li^+ exchange reaction on the surface of LNCM electrode enhanced the reduction ability of oxygen that released in the initial charge process.[42] What is more, PANI coating layer optimized the electrochemical catalytic conditions of the interface between particle surfaces and electrolyte. Fig. 9b shows the comparison of the discharge open-circuit voltage of the electrodes. The smaller discharge voltage drops for the cells with PANI-coated electrodes reflect that PANI coating layer has reduced the internal resistance of the cell system, which contributes to the following cycle stability.

The cycling performance of the pristine LNCM and PANI-coated LNCM at the current density of 25 mA g^{-1} (0.1 C) is shown in Fig. 10. PANI-coated LNCM electrodes exhibit excellent cycle stability after five cycles of activating at 12.5 mA g^{-1} (0.05 C). The sharp drop of the discharge capacity after five cycles is caused by the changes of the current density. The discharge capacity of the electrodes are still retained at 209.1 mA h g^{-1}/PI1, 282.1 mA h g^{-1}/PI2, 260.2 mA h g^{-1}/PI3, 213.6 mA h g^{-1}/P4 and 196.4 mA h g^{-1}/PI5 with the coulombic efficiency of 59.90%, 80.60%, 73.46%, 60.96% and 55.56% (relative to the initial discharge capacity) after 80 cycles, respectively. However, the pristine LNCM retains its

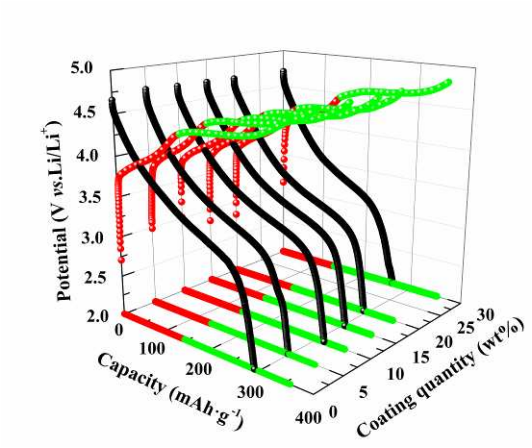

Fig. 8 Initial charge-discharge performance of the prepared samples at low rate (0.05 C).

discharge capacity at 187.7 mA h g^{-1} with the coulombic efficiency of 52.28% after the same cycles. High rate cycling performance of the prepared samples is shown in Fig. S3†, further proving PANI coating layer improves the cycle stability at high rate (1C).

The morphology observation of the cycled pristine electrode was compared with PANI-coated electrode by HRTEM, as shown in Fig. 11. The original distinct crystal faces and boundaries of $Li[Li_{0.2}Mn_{0.54}Ni_{0.13}Co_{0.13}]O_2$ particles become uneven with the remarkable eroded traces (Fig. 11a), which is possibly caused by the erosion of HF during the cyclic process.[62] The (003) lattice fringes are twisty and discontinuous (Fig. 11b), accompanying with the polycrystalline structure on the surface of $Li[Li_{0.2}Mn_{0.54}Ni_{0.13}Co_{0.13}]O_2$ particles (Fig. 11c). On the contrary, the PANI-coated electrode does not present obvious structural damage. After 100 cycles at the current density of 25 mA g^{-1}, the PANI coating layer reserved steadily on the surface of $Li[Li_{0.2}Mn_{0.54}Ni_{0.13}Co_{0.13}]O_2$ particles (Fig. 11d). There are no changes of the straight lattice fringes (003) under the protection of PANI coating layer (Fig. 11e). Therefore, the thin PANI coating layer shows its advantages in maintaining the integrity of surface material crystal structure, which is necessary for the excellent

Table 3 The detailed charge-discharge values of $Li[Li_{0.2}Mn_{0.54}Ni_{0.13}Co_{0.13}]O_2$ before and after polyaniline coating.

Samples	Initial charge capacity(mA h g^{-1})	Initial discharge capacity(mA h g^{-1})	Charge capacity below 4.4 V (mA h g^{-1})	Charge capacity between 4.4 V and 4.6V (mA h g^{-1})
LNCM	359.0	291.9	145.3	170.2
PI1	349.1	298.3	145.6	164.8
PI2	352.2	313.5	146.5	158.5
PI3	354.2	303.7	148.7	162.0
PI4	350.4	292.8	144.7	163.4

PI5	353.5	261.6	148.1	117.8

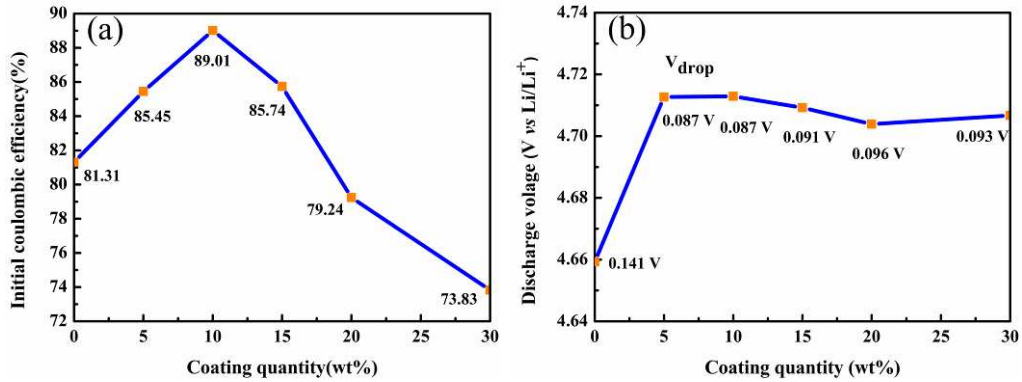

Fig. 9 Initial coulombic efficiency (a) and discharge open-circuit voltage of the prepared samples (b).

cycling performance.

The corresponding differential capacity (dQ/dV) curves of the pristine LNCM and PANI-coated LNCM (PI2) have been evaluated at different cycles, as illustrated in Fig. 12. During the initial charge process, two obvious anodic peaks appear around 4.0 V and 4.5 V (*vs*. Li/Li$^+$). The prior peak at 4.0 V attributes to the oxidation of Co^{3+}/Co^{4+} and $Ni^{2+}/Ni^{3+}/Ni^{4+}$ accompanying with the deintercalation of lithium ion from crystal phase $LiMO_2$ (M=Ni, Co, Mn),[63] while the other anodic peak at 4.5 V relates to the oxygen loss with the activation of the transfer metal manganese.[64] In the initial discharge process, only one cathodic peak appears around 3.3 V which is attributed to the reduction of $Ni^{4+}/Ni^{3+}/Ni^{2+}$ and Co^{4+}/Co^{3+} with the lithium ion intercalating back into lithium vacancy. The reduced anodic peak intensity around 4.5 V after PANI coating illustrates that oxygen loss in the initial charge process is partly suppressed by the PANI coating layer, from which we surmise that the special hydrogen bond between the polar oxygen and hydrogen (on the amidogen) provides the binding force to oxygen. In the following cycles, a cathodic peak is loaded around 2.9 V corresponding to the reduction of the activated tetravalent manganese (Mn^{4+}/Mn^{3+}) with the anodic peak at around 3.3 V.[62] The dissolution of bivalent manganese ion into the electrolyte (Eq. 5) and Jahn–Teller distortion during redox reaction of the activated manganese affect the cycle stability of the pristine LNCM.[65]

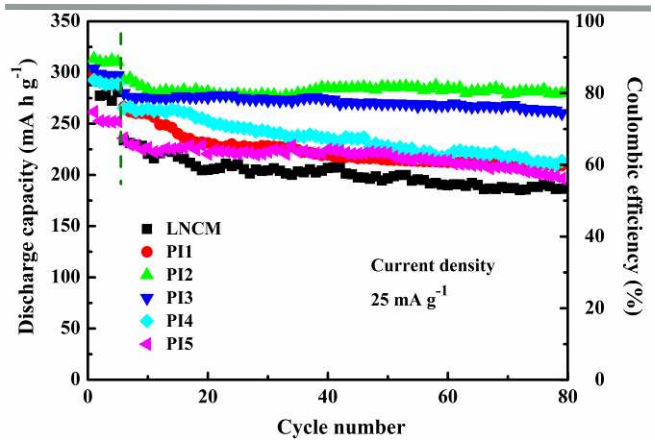

Fig. 10 Cycling performance and coulombic efficiency of the pristine LNCM and PI2 at the current density of 25 mA g^{-1}.

$$2Mn^{3+}_{(solid)} \rightarrow Mn^{4+}_{(solid)} + Mn^{2+}_{(liquid)} \quad (5)$$

What is interesting, activation of the tetravalent manganese is proved to be a gradual process. The distinct reduction peak of the activated manganese appears during the third discharge process

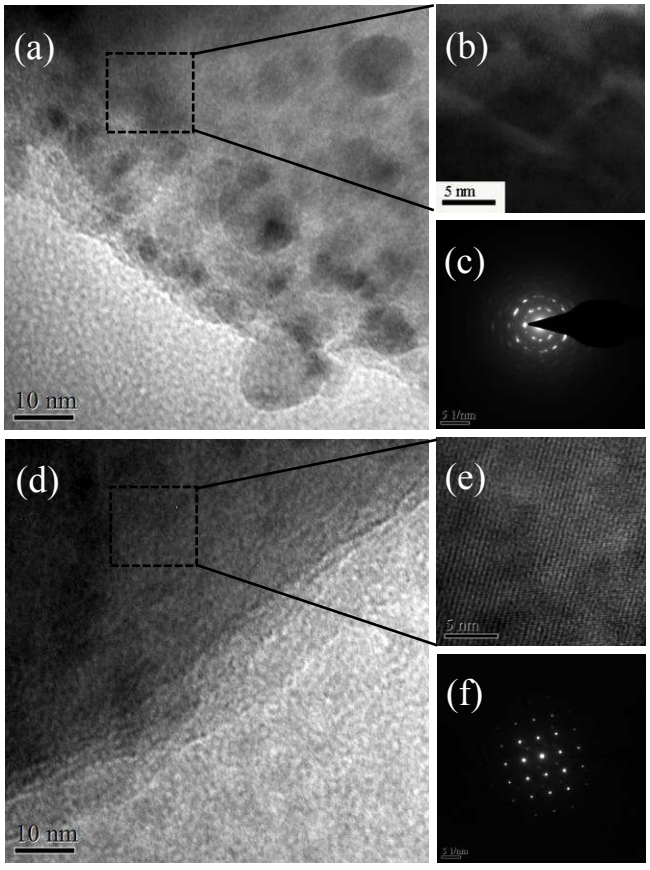

Fig. 11 HRTEM images of (a), (b) the pristine electrode after 100 cycles at 0.1 C; (c) electron diffraction of the pristine electrode; HRTEM images of (d), (e) the PANI-coated electrode (PI2) after 100 cycles at 0.1 C; (f) electron diffraction of the PANI-coated electrode (PI2).

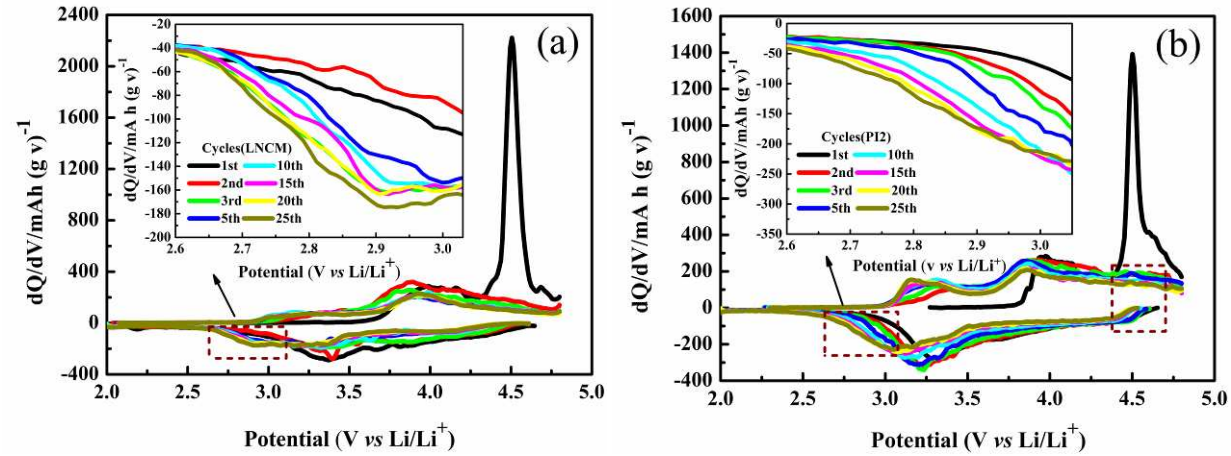

Fig. 12 The differential capacity vs. voltage curves of (a) the pristine electrode and (b) PANI-coated electrode (PI2).

(Fig. 12a, insert). However, the PANI layer slows down the activation of manganese in the charge-discharge cycles (Fig. 12b, insert), the anodic peak around 4.5 V disappears after five cycles as signed in the rectangle. This moderate way of oxygen loss and manganese activation has reduced the impact on the crystal structure.

The high rate discharge capacity of the pristine LNCM and PANI-coated LNCM at different rates range 0.05 C (12.5 mA g^{-1}) - 10 C (2500 mA g^{-1}) for each six cycles are shown in Fig. 14. Obviously, surface modification with PANI has improved the fast discharge capability of $Li[Li_{0.2}Mn_{0.54}Ni_{0.13}Co_{0.13}]O_2$ at high current densities. The maximum discharge capacity is 198.6 mA h g^{-1} at 10 C (PI2) with the capacity retention of 63.35% in comparison with the capacity at a low rate of 0.05 C. The coating quantity has great impact on the high rate performance of PANI-coated LNCM. As a kind of electronic conductive polymers, polyaniline coating layer doped with proton acid accelerates the electronic transmission on the surface of LNCM particles and shortens the activation process (Fig. 13 insert), which is induced by the insulating Li_2MnO_3 component.[66] However, thick coating layer will hinder the deintercalate/intercalate efficiency on the surface of LNCM particles. According to the electrochemical performance, PI2 exhibits the most ideal coating features.

Electrochemical impedance spectra (EIS) of the pristine LNCM and PANI-coated LNCM (PI2) are measured to investigate the origin of the improvement in rate capability of PANI-coated LNCM preferably. The Nyquist plots of the pristine electrode and PI2 electrode measured after the 1st, 10th, 20th, 50th cycles are shown in Fig. 14. The similar Nyquist plots include two semicircles and a long slash under the fully discharge stages. The high-frequency semicircle represents the migration of lithium ion through the interfacial film, and the intermediate-frequency semicircle is related to the charge transfer reaction on the electrode/electrolyte interface. While the low-frequency slash refers to the semi-infinite lithium ion diffusion process in the bulk. Table 4 shows the fitting EIS spectra values by using the equivalent circuit model. As shown in Fig. 14c, R_s, R_{sf} and R_{ct} represent the electrolyte resistance between the reference electrode and working electrode, the surface film resistance of the surface layer and the charge-transfer resistance of the surface electrochemical reaction, respectively. Meanwhile, CPEs and Z_w mean the corresponding constant phase elements and the Warburg impedance.[67] It is obvious that PANI coating layer has improved the conducting conditions of the pristine electrode interface. After the initial cycle, the pristine electrode possesses higher surface film resistance than that of the PANI-coated electrode, indicating that the formation of SEI layer is suppressed by PANI coating layer in the initial cycle. In the following cycles, the values of R_{sf} are dramatically increased for the pristine electrode, while PANI-coated electrode maintains the stabilized values around 7.15 Ω. The charge-transfer resistance of the pristine electrode increase from 102.71 Ω at the initial cycle to 505.47 Ω after 50 cycles, but in contrast the R_{ct} values of the PANI-coated electrode increase from 80.42 Ω to 134.82 Ω at the corresponding cycles. Therefore, the improved interfacial electrochemical reaction activity has enhanced the cycle stability and high rate capacity of PANI coated-LNCM electrode.

As investigated above, the composite modified LNCM shows greater improvement in electrochemical properties than that of the layered solid solution cathode materials undergone conventional modification, especially in high rate capacity and cycle stability.[68,69] H^+/Li^+ exchange reaction on the surface of LNCM provides the optimized internal diffusion path of Li^+ and enhances the reduction ability of oxygen that released in the initial charge process, resulting in the high initial coulombic efficiency of 89.01%. In the initial charge-discharge cycle, formation of the SEI film is suppressed under the protection of the ultra-thin PANI

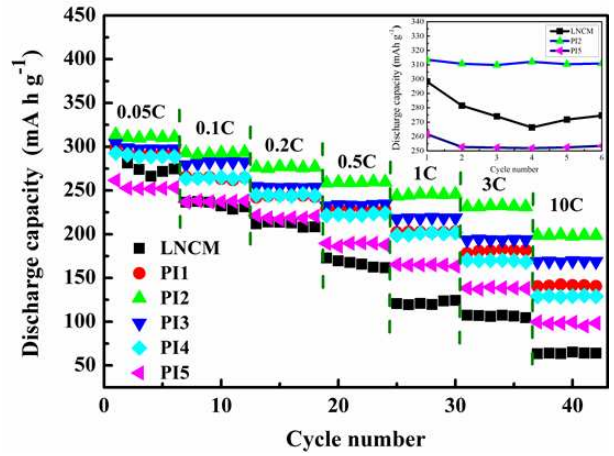

Fig. 13 High rate performance of the pristine and PANI-coated samples, insert: the first six cycles of the pristine, PI2 sample and PI5 sample.

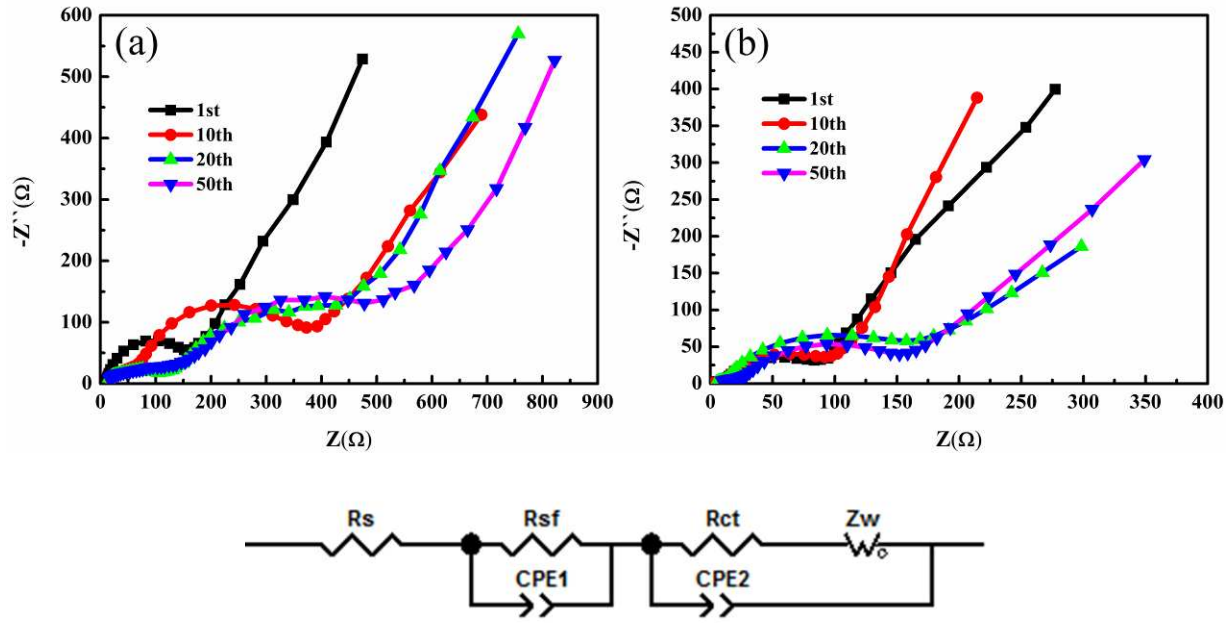

Fig. 14 Electrochemical impedance spectra of (a) the pristine LNCM and (b) PANI-coated LNCM (PI2) after the 1st, 10th, 20th, 50th cycles; (c) the equivalent circuit model used for curve fitting.

coating layer, which is important for the stability of the broadened diffusion path of Li^+ in the continuous charge-discharge cycles. Meanwhile, the ultra-thin PANI coating layer on the surface of the PANI-coated $Li[Li_{0.2}Mn_{0.54}Ni_{0.13}Co_{0.13}]O_2$ maintains the integrity of the elements and surface material crystal structure by protecting the electrode from hydrofluoric acid erosion. Moreover, the special interfacial interaction between PANI layer and the $Li[Li_{0.2}Mn_{0.54}Ni_{0.13}Co_{0.13}]O_2$ particle surface reduces the release of oxygen. Thickness of the coating layer is crucial to the electrochemical properties of the surface modified electrode materials. At low coating amounts, the thin PANI layer increases the interfacial electrochemical reaction activity greatly by promoting the interfacial electronic conductivity. However, with the increasing of coating amount, the lithium transfer efficiency through the interfacial film could be hindered due to the thick coating layer. Therefore, the PANI surface modification with composite impact is efficient to optimize the interfacial electrochemical reaction environment, leading to the enhanced electrochemical properties.

Conclusions

The lithium-rich layered $Li[Li_{0.2}Mn_{0.54}Ni_{0.13}Co_{0.13}]O_2$ was synthesized by a fast co-precipitation method, and surface modified successfully by PANI (5 wt%, 10 wt%, 15 wt%, 20 wt%, 30 wt% theoretically) via in-situ chemical oxidation polymerization in the acid medium. The PANI-coated $Li[Li_{0.2}Mn_{0.54}Ni_{0.13}Co_{0.13}]O_2$ retained the typical layered hexagonal structure of α-$NaFeO_2$, accompanying with slightly increasing of unit-cell parameter c in the special acid leaching procedure. The amorphous PANI coating layer maintained the integrity of surface material crystal structure of the $Li[Li_{0.2}Mn_{0.54}Ni_{0.13}Co_{0.13}]O_2$ particles in the continuous charge-discharge cycles. The PANI-coated samples present great improvements in initial coulombic efficiency, high-rate capacity and cycle stability by enhancing the reduction ability of oxygen that released in the initial charge process, slowing down the dissolution of transfer metal and optimizing the interfacial electrochemical reaction activity. Conducting polymer coating by in-situ chemical oxidation polymerization in the acid medium not only broadened the diffusion path of lithium ions in the special acid leaching process, but also the stable conducting polymer layer will protect the electrodes from external erosion. Therefore, the compound modification of surface coating and acid treatment is proved to be an ideal way to improve the electrochemical performance of the lithium-rich layered solid solution materials. The application of conducting polymers in energy storage areas is meaningful to develop new modified or composited electrode materials for advanced energy storage devices.

Table 4 The fitted values of R_s and R_{ct} for the pristine LNCM and PANI-coated LNCM after the 1st, 10th, 20th, 50th cycles.

Sample	LNCM		PI2	
	R_{sf}	R_{ct}	R_{sf}	R_{ct}
1st	17.58	102.71	7.04	80.42
10th	64.52	316.83	7.15	90.18
20th	83.47	387.19	7.19	129.71
50th	92.76	505.47	7.16	134.82

Acknowledgements

The project was supported by the National Natural Science Foundation of China (51172023, 51372021) and the National High Technology Research and Development Program of China (863) (2012AA110302).

Notes and references

[a] State Key Laboratory of Advanced Metallurgy, University of Science and Technology Beijing, No. 30 College Road, Haidian District, Beijing 100083, China.
[b] Lab of Advanced Materials, Department of Materials Science and Engineering, Tsinghua University, Beijing 100084, China.
† ESI

1 M. Armand and J. M. Tarascon, *Nature*, 2008, **451**,652.
2 J. B. Goodenough and Y. Kim, *Chem. Mater.*, 2010, **22**, 587.
3 M. M. Thackeray, C. Wolverton and E. D. Isaacs, *Energy Environ Sci.*, 2012, **5**, 7854.
4 B. Dunn, H. Kamath and J. M. Tarascon, *Science*, 2011, **334**, 928.
5 P. S. Maram, G. C. Costa and A. Navrotsky, *Angew. Chem.*, 2013, **52**, 12139.
6 A. Sakuda, N. Nakamoto, H. Kitaura, A. Hayashi, K. Tadanaga and M. Tatsumisago, *J. Mater. Chem.*, 2012, **22**, 15247.
7 L. X. Yuan, Z. H. Wang, W. X. Zhang, X. L. Hu, J. T. Chen, Y. H. Huang and J. B. Goodenough, *Energy Environ Sci.*, 2011, **4**, 269.
8 Q. Shi, L. Xue, Z. Wei, F. Liu, X. Du and D. D. DesMarteau, *J. Mater. Chem. A*, 2013, **1**, 15016.
9 J. Wang, J. Yang, Y. Tang, R. Li, G. Liang, T.-K. Sham and X. Sun, *J. Mater. Chem. A,* 2013, **1**, 1579.
10 J. Wang, Q. Zhang, X. Li, Z. Wang, H. Guo, D. Xu and K. Zhang, *Phys. Chem. Chem. Phys.*, 2014, **16**, 16021.
11 D. Guan, J. A. Jeevarajan and Y. Wang, *Nanoscale*, 2011, **3**, 1465.
12 Y. Dai, L. Cai and R. E. White, *J. Electrochem. Soc.*, 2012, **160**, A182.
13 W. H. Ryu, D. H. Kim, S. H. Kang and H. S. Kwon, *RSC Adv.*, 2013, **3**, 8527.
14 Q. Y. Wang, J. Liu, A. V. Murugan and A. Manthiram, *J. Mater. Chem.*, 2009, **19**, 4965.
15 X. Yang, X. Wang, Q. Wei, H. Shu, L. Liu, S. Yang, B. Hu, Y. Song, G. Zou, L. Hu and L. Yi, *J. Mater. Chem.*, 2012, **22**, 19666.
16 B. Ammundsen and J Paulsen, *Adv. Mater.*, 2001, **13**, 943.
17 Y. N. Jo, K. Prasanna, S. J. Park and C. W. Lee, *Electrochimica. Acta*, 2013, **108**, 32.
18 F. Li, S. X. Zhao, K. Z. Wang, B. H. Li and C. W. Nan, *Electrochimica. Acta*, 2013, **97**, 17.
19 N. Yabuuchi, K. Yoshii, S. T. Myung, I. Nakai and S. Komaba, *J. Am. Chem. Soc.*, 2011, **133**, 4404.
20 D. Mohanty, A. S. Sefat, S. Kalnaus, J. Li, R. A. Meisner, E. A. Payzant, D. P. Abraham, D. L. Wood and C. Daniel, *J. Mater. Chem. A*, 2013, **1**, 6249.
21 P. Lanz, H. Sommer, M. Schulz-Dobrick and P. Novák, *Electrochimica. Acta*, 2013, **93**, 114.
22 S. F. Amalraj, D. Sharon, M. Talianker, C. M. Julien, L. Burlaka, R. Lavi, E. Zhecheva, B. Markovsky, E. Zinigrad, D. Kovacheva, R. Stoyanova and D. Aurbach, *Electrochimica. Acta*, 2013, **97**, 259.
23 C. Jacob, J. Jian, Y. Zhu, Q. Su and H. Wang, *J. Mater. Chem. A*, 2014, **2**, 2283.
24 B. Song, M. O. Lai, Z. Liu, H. Liu and L. Lu, *J. Mater. Chem. A*, 2013, **1**, 9954.
25 I. T. Kim, J. C. Knight, H. Celio and A. Manthiram, *J. Mater. Chem. A*, 2014, **2**, 8696.
26 Y. K. Sun, M. J. Lee, C. S. Yoon, J. Hassoun, K. Amine and B. Scrosati, *Adv. Mater.*, 2012, **24**, 1192.
27 A. Dianat, N. Seriani, M. Bobeth and G. Cuniberti, *J. Mater. Chem. A*, 2013, **1**, 9273.
28 S. Laha, E. Morán, R. Sáez-Puche, M. Á. Alario-Franco, A. J. Dos. santos-Garcia, E. Gonzalo, A. Kuhn, S. Natarajan, J. Gopalakrishnan and F. García-Alvarado, *J. Mater. Chem. A*, 2013, **1**, 10686.
29 S. K. Martha, J. Nanda, Y. Kim, R. R. Unocic, S. Pannala and N. J. Dudney, *J. Mater. Chem. A*, 2013, **1**, 5587.
30 S. H. Kang, C. S. Johnson, J. T. Vaughey, K. Amine and M. M. Thackeray, *J. Electrochem. Soc.*, 2006, **153**, A1186.
31 D. Y. W. Yu, K. Yanagida and H. Nakamura, *J. Electrochem. Soc.*, 2010, **157**, A1177.
32 Y. Deng, S. Liu and X. Liang. *J Solid State Electrochem*, 2013, **17**,1067.
33 L. N. Cong, X. G. Gao, S. C. Ma, X. Guo, Y. P. Zeng, L. H. Tai, R. S. Wang, H. M. Xie and L. Q. Sun, *Electrochimica. Acta*, 2014, **115**, 399.
34 Q. Q. Qiao, H. Z. Zhang, G. R. Li, S. H. Ye, C. W. Wang and X. P. Gao, *J. Mater. Chem. A*, 2013, **1**, 5262.
35 S. H. Kang and M. M. Thackeray, *Electrochem. Commun*, 2009, **11**, 748.
36 S. H. Guo, H. J. Yu, P. Liu, X. Z. Liu, D. Li, M. W. Chen, M. Ishida and H. S. Zhou, *J. Mater. Chem. A*, 2014, **2**, 4422.
37 D. Guan, J. A. Jeevarajan and Y. Wang, *Nanoscale*, 2011, **3**, 1465.
38 H. M. Wu, I. Belharouak, A. Abouimrane, Y. K. Sun and K. Amine, *J. Power Sources*, 2010, **195**, 2909.
39 S. J. Shi, J. P. Tu, Y. J. Zhang, Y. D. Zhang, X. Y. Zhao, X. L. Wang and C. D. Gu, *Electrochimica. Acta*, 2013, **108**, 441.
40 J. Liu and A. Manthiram, *Chem. Mater.*, 2009, **21**, 1695.
41 J. S. Kim, C. S. Johnson, J. T. Vaughey and M. M. Thackeray, *J. Power Sources*, 2006, **153**, 258.
42 G. Xu, J. Li, Q. Xue, X. Ren, G. Yan, X. Wang and F. Kang, *J. Power Sources*, 2014, **248**, 894.
43 Y. G. Wang, Y. R. Wang, E. Hosono, K. X. Wang and H. S. Zhou, *Angew. Chem. Int. Ed.*, 2008, **47**, 7461.
44 J. K. Kim, J. Manuel, M. H. Lee, J. Scheers, D. H. Lim, P. Johansson, J. H. Ahn, A. Matic and P. Jacobsson, *J. Mater. Chem.*, 2012, **22**, 15045.
45 K. S. Park, S. B. Schougaard and J. B. Goodenough, *Adv. Mater.*, 2007, **19**, 848.
46 C. P. Fonseca and S. Neves, *J. Power Sources*, 2004, **135**, 249.
47 K. Karthikeyan, S. Amaresh, V. Aravindan, W. S. Kim, K. W. Nam, X. Q. Yang and Y. S. Lee, *J. Power Sources*, 2013, **232**, 240.
48 L. Chen, L. J. Sun, F. Luan, Y. Liang, Y. Li and X. X. Liu, *J. Power Sources*, 2010, **195**, 3742.
49 N. Ashok Kumar and J. B. Baek, *Chem. Commun.*, 2014, **50**, 6298.
50 Y. Chen, G. Xu, J. Li, Y. Zhang, Z. Chen and F. Kang, *Electrochimica. Acta*, 2013, **87**, 686.
51 M. Gu, I. Belharouak, J. Zheng, H. Wu, J. Xiao, A. Genc, K. Amine, S. Thevuthasan, D. R. Baer, J. G. Zhang, N. D. Browning, J. Liu and C. Wang, *ACS nano*, 2013, **7**, 760.
52 B. Song, M. O. Lai, Z. Liu, H. Liu and L. Lu, *J. Mater. Chem. A*,2013, **1**, 9954.
53 J. Liu and A. Manthiram. *J. Mater. Chem.*, 2010, **20**, 3961.
54 C. Venkateswara Rao, J. Soler, R. Katiyar, J. Shojan, W. C. West and R. S. Katiyar, *J. Phys. Chem. C*, 2014, **118**, 14133.

55 N. Yabuuchi, K. Yoshiii, S. T. Myung, L Nakai and S. Komaba, *J. Am. Chem. Soc.*, 2011, **133**, 4404.
56 A. Rougier, P. Gravereau and C. Delmas, *J. Electrochem. Soc.*, 1996, **143**, 1168.
57 S. C. Yin, Y. H. Rho, I. Swainson and L. F. Nazar, Chem. Mater., 2006, **18**, 1901.
58 W. Chen, R. B. Rakhi and H. N. Alshareef, *J. Mater. Chem. A*, 2013, **1**, 3315.
59 Z. Q. Tong, Y. N. Yang, J. Y. Wang, J. P Zhao, B. L. Su and Y. Li, *J. Mater. Chem. A*, 2014, **2**, 4642.
60 W. B. Stockton and M. F. Rubner, *Macromolecules*, 1997, **30**, 2717.
61 S. H. Kang, P. Kempgens, S. Greenbaum, A. J. Kropf, K. Amine and M. M. Thackeray, *J. Mater. Chem.*, 2007, **17**, 2069.
62 S. T. Myung, K. Izumi, S. Komoba, Y. K. Sun, H. Yashiro and N. Kumagai, *Chem. Mater*., 2005, **17**, 3695.
63 A. R. Armstrong, M. Holzapfel, P. Novák, C. S. Johnson, S. H. Kang, M. M. Thackeray and P. G. Bruce, *J. Am. Chem. Soc.*, 2006, **128**, 8694.
64 D. Mohanty, A. S. Sefat, S. Kalnaus, J. Li, R. A. Meisner, E. A. Payzant, D. P. Abraham, D. L. Wood and C. Daniel, *J. Mater. Chem. A*, 2013, **1**, 6249.
65 J. Ma, Y. N. Zhou, Y. R. Gao, Q. Y. Kong, Z. X. Wang, X. Q. Yang and L. Q. Chen, *Chem. Eur. J.,* 2014, **20**, 8723.
66 C. S. Johnson, N. C. Li, C. Lefief, J. T. Vaufhey and M. M. Thackeray, Chem. Mater., 2008, **20**, 6095.
67 X. J. Yang, T. Yang, S. S. Liang, X. Wu and H. P. Zhang, J. Mater. Chem. A, 2014, **2**, 10359.
68 C. Wu, X. Fang, X. Guo, Y. Mao, J. Ma, C. Zhao, Z. Wang and L. Chen, *J. Power Sources*, 2013, **231**, 44.
69 X. Liu, J. Liu, T. Huang and A. Yu, *Electrochimica. Acta*, 2013, **109**, 52.

Table of contents entry

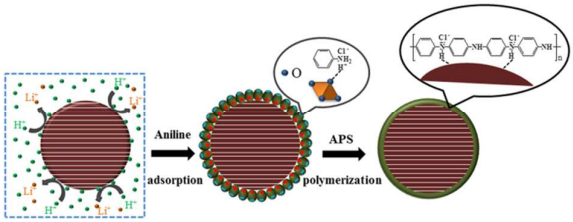

TOC:

Compound modification of polyaniline coating and acid treatment is an ideal way to improve the electrochemical performance of $Li[Li_{0.2}Mn_{0.54}Ni_{0.13}Co_{0.13}]O_2$.